JJEE
Volume X | Number X | Month 20XX | Pages XXX-XXX

Jordan Journal of Electrical Engineering

ISSN (print): 2409-9600, ISSN (online): 2409-9619

Homepage: jjee.ttu.edu.jo

A Robust Backstepping Controller Based on Nonlinear Observer for Shunt Active Filters to Improve Power Quality in Four-Wire Distribution Systems

Parisa Sarafrazi[1], Seyed Abbas Taher[2*], Ali Akhavan[3]

[1, 2] Faculty of Electrical and Computer Engineering, University of Kashan, Kashan, Iran
E-mail: sataher@kashanu.ac.ir
[3]AAU Energy, Aalborg University, Aalborg, Denmark

Received: Nov 19, 2023 *Revised: Mar 01, 2024* *Accepted: Mar 07, 2024* *Available online: Aug 19, 2024*

***Abstract*—** This article introduces a novel approach to enhance the performance of LCL based active power filters (APFs) in four-wire distribution systems by employing a nonlinear current control strategy. The strategy combines backstepping control (BSC) and a nonlinear disturbance observer (NDOB) to effectively manage harmonic and interharmonic grid currents. By situating the shunt active power filter (SAPF) at the point of common coupling (PCC) via the LCL filter, the technique ensures that grid connected currents remain balanced and purely sinusoidal. The integration of NDOB with BSC aims to fortify the resilience of BSC against disturbances. Consequently, any disturbances occurring within the system are precisely estimated by the NDOB and subsequently mitigated through the BSC mechanism. Notably, this approach showcases robust adaptability across diverse scenarios, encompassing external disturbances, variations in filter parameters, nonlinear loads laden with harmonics and interharmonics, load imbalances, and non-ideal grid voltages. Its performance remains robust and stable even when disturbances are present. Comparative analysis with linear-based methodologies underscores the advantages of this approach, revealing quicker and smoother transient responses. The efficacy of the proposed technique is demonstrated through comprehensive simulation studies, substantiating its potential for significantly advancing power quality in complex distribution systems.

***Keywords*—** Harmonic and interharmonic grid currents; Backstepping control; Nonlinear disturbance observer; Active power filter; Four-wire distribution system; Power quality.

Nomenclature

BSC	Backstepping Control
BS-DPC	Backstepping direct power control
DFIG	Dual fed induction generator
DG	Distributed generation
GM	Gain margin
NDOB	Nonlinear Disturbance Observer
PCC	Point of common coupling
PI	Proportional-integral
PM	Phase margin
PPF	Passive power filters
PR	Proportional-resonant
PV	Photovoltaic
RC	Repetitive Controller
SAPF	Shunt Active Power Filter
SMC	sliding mode control
THD	Total Harmonic Distortion
GM	Gain margin
C_{dc1}, C_{dc2}	DC link capacitor
f_s	Sampling frequency
f_{sw}	Switching Frequency
H_1, H_2, H_3	BS parameters
k_{Rh}	Resonant gain
k_1, k_2	NDOB parameters
k_p, k_I	PI controller gain
PM	phase margin
R/L	Nonlinear load
R_L	Linear load
R_I/L_I	Inverter side impedance
R_g/L_g	Grid side impedance
V_{dc}	DC link reference voltage

* Corresponding author
DOI: https://doi.org/10.5455/jjee.204-1700421844

1. INTRODUCTION

The nonlinear loads stand out as the primary culprits behind the emergence of both harmonics and interharmonics within the grid infrastructure. The escalating utilization of such nonlinear loads has significantly eroded the overall power quality landscape. The repercussions of these harmonics are notably detrimental, leading to issues like signal interference, device breakdowns, overheating, equipment malfunctions, and overvoltage occurrences [1].

Interharmonics, on the other hand, stems from loads that do not oscillate synchronously with the fundamental frequency of the power system. A prominent origin of interharmonics arises from power electronic components that bridge two AC systems operating at disparate frequencies through a DC link, thereby generating these unwanted frequency components [1]. Instances include loads encompassing cycloconverters, speed regulated drives for both synchronous and induction motors, as well as arc furnaces. The presence of interharmonics within the power network engenders a suite of challenges, extending beyond those posed by harmonics alone. Consequences encompass phenomena such as flickering, interference with control systems, disruption of protection signals, current transformer saturation, voltage fluctuations, and incorrect system operations [2]. Hence, the critical imperative of devising effective compensation techniques to ameliorate these adverse impacts and elevate power quality standards.

Passive power filters (PPF) find utility in mitigating harmonics originating from nonlinear loads within the grid current [3]. Characterized by a straightforward design approach and economical construction, passive filters exhibit notable cost-effectiveness. However, their susceptibility to inducing resonances with grid impedance [4] underscores the preference for active power filters (APFs) as a more judicious solution. The realm of active power filter control methods encompasses a diverse array, and the selection of an appropriate approach significantly influences the filter's efficacy in compensation These methods can be broadly categorized into two groups. The first group involves strategies that entail designing distinct controllers for individual harmonic orders, often relying on proportional-integral (PI) or proportional-resonant (PR) controllers [5, 6]. In contrast, the second group embraces techniques that obviate the need for dedicated controller design. Notable examples comprise sliding mode control (SMC) [7, 8], predictive control [9, 10], repetitive control [11, 12], deadbeat control [13, 14], fuzzy control [15, 16], and neural network control [17, 18]. This second category boasts a computational advantage over the first, characterized by lower computational loads.

Among these methods, the repetitive control (RC) approach is specifically designed to accurately track periodic reference signals and eliminate periodic disturbances [19]. Reference [20] proposed an algorithm that utilizes repetitive control for adaptive correction of virtual impedance. The objective of this algorithm is to suppress grid voltage harmonics. In [21], a deadbeat control scheme that incorporates repetitive control is proposed to enhance the dynamic performance of the control system. Moreover, the RC method can be combined with other controller topologies to create highly efficient and high-performance control structures, as demonstrated in references [22] and [23]. The RC method operates by rejecting harmonics that are integer multiples of the main frequency. Therefore, if there is a deviation in the main frequency, RC will not be able to eliminate the harmonics. To solve this problem, the variable sampling rate approach has been proposed [24]. Another similar method is the fractional delay approach, which uses a finite impulse response (FIR) filter based on Lagrange interpolation to model the fractional part [25]. However, variable sampling rate methods lead to large changes

in system dynamics and impose a fractional delay in many mathematical calculations [26]. The predictive and deadbeat control methods have the characteristics such as high accuracy, small steady-state error, relatively simple control, unlimited bandwidth, and fast dynamic response [27]. However, parameter uncertainty and delay in the digital implementation of the control system can limit the performance improvement of these control techniques, as mentioned in reference [28]. In [29], an improved deadbeat current controller is used for the LC hybrid shunt active power filter to reduce harmonics and reactive power in the system. Another method is the sliding mode method. Unlike repetitive and predictive methods, this method does not depend on an accurate model, so it is suitable for controlling systems with parameter uncertainties [30]. However, the SMC method suffers from a chattering phenomenon due to high-frequency switching in the control signal. To solve this problem, an adaptive SMC (ASMC) is proposed in [31] and a complementary sliding mode control (CSMC) method is proposed in [32]. However, the sliding mode controller must continuously increase the switching power to maintain stability in the presence of disturbances. This reduces the effectiveness of the umbrella attenuation method. [33]. In [34], a new intelligent SMC is proposed to increase the accuracy and reduce the effect of disturbances in the system. The disadvantage of this method is its complexity.

Hence, the adoption of backstepping control (BSC) has garnered significant attention for managing nonlinear systems, attributed to its manifold benefits. The backstepping approach, akin to sliding mode control, employs a Lyapunov based recursive design methodology, seamlessly transforming the task of designing high order systems into a series of challenges pertaining to lower order systems [35]. This methodology finds widespread application across diverse domains. For instance, in [36], a backstepping direct power control (BS-DPC) strategy is introduced to oversee a dual-fed induction generator (DFIG) across balanced and unbalanced network scenarios. Another study, outlined in [37], proposes a sensorless DC-link voltage controller utilizing the backstepping framework for a single-phase shunt active power filter (SAPF). This application employs backstepping to estimate the DC link voltage, subsequently regulated using a PI controller. Meanwhile, in [38], backstepping control is harnessed to manage the DC link voltage within a SAPF, yielding superior response speed in comparison to a PI controller. In the realm of photovoltaic (PV) systems, [39] delves into the design of a BSC method, although its resilience in the face of parameter uncertainties remains unverified. Reference [40] proposes a robust control based on integrated back-end control (IBC) to improve the power quality of a microgrid-connected photovoltaic (PV) system with battery energy storage systems. Similarly, [41] presents a BS-DPC strategy for governing an AC/DC converter connected to the grid, showcasing commendable dynamic performance in the context of unbalanced grid conditions. However, the assessment of the control system's performance in the presence of parameter uncertainties and system disturbances remains unexplored.

While the conventional BSC methodology offers advantages through its simplicity and adaptable design, it inherently lacks robustness when faced with system uncertainties and external disruptions. An effective approach addressing this concern is the application of adaptive backstepping control, which represents a refined variation of traditional backstepping control, incorporating the estimation of elusive system parameters. For instance, in [42], an adapted version of BSC is proposed to govern grid connected photovoltaic (PV) systems, overseeing both DC link voltage and AC-side currents. Leveraging an adaptive law rooted in Lyapunov stability theory, this approach strives to estimate uncertain parameters within the

grid connected inverter. Nonetheless, the scheme's resilience against external disturbances remains unverified. In a separate context, [43] explores the fusion of backstepping methodology with sliding mode control to regulate grid connected distributed generation (DG) systems, specifically for compensating interharmonic loads. Here, disturbances within the system are estimated through SMC and subsequently counteracted via the backstepping method. However, the adoption of the SMC technique introduces an issue of chattering, detracting from the method's effectiveness. Additionally, it's noteworthy that the interharmonic load presented in [43] is treated as a current source, which might not capture all potential scenarios accurately.

This paper presents a novel and robust approach that integrates nonlinear backstepping control with a nonlinear disturbance observer (NDOB) to effectively regulate shunt active power filters. The primary objective is to achieve compensation for both harmonic and, notably, interharmonic disturbances in the presence of uncertainties and external perturbations. The study focuses on a four-wire distribution system, where the mitigation of imbalances is also addressed. The proposed methodology is designed to assimilate the impact of disturbances into a coherent framework, treating them as an integrated entity. The NDOB is then employed to accurately estimate these disturbances, subsequently rectified through the implementation of the backstepping control (BSC) technique. Ensuring system stability, the proposed control scheme's asymptotic stability is scrutinized following the tenets of the Lyapunov stability criterion, thereby ensuring the system's convergence and stability. It is anticipated that the application of the proposed method to shunt active filters will yield substantial robustness against unknown parameters and external disturbances. This heightened robustness enhances compensation accuracy, effectively counteracting filter parameter uncertainties and external disruptions. Furthermore, the inclusion of this estimation mechanism eliminates the necessity for additional sensors and telecommunication links, resulting in increased compensation precision and reduced measurement errors, ultimately leading to cost savings. Of significance is the exploration of interharmonic load compensation, an area that has garnered limited research attention. The study delves into an interharmonic load scenario, specifically focusing on an induction motor speed control drive. The proposed approach is benchmarked against the well-established proportional-resonant (PR) control technique. Comprehensive testing encompasses diverse scenarios, including the presence of nonlinear loads generating harmonic and interharmonic currents, load imbalances, weak grid conditions, external disturbances, and variations in filter parameters. The comparative analysis extends beyond steady state responses, encompassing transient behaviors of both controllers. Simulation results conducted using MATLAB/Simulink provide compelling validation for the superiority of the backstepping method. The proposed approach demonstrates its potential to markedly enhance control performance in the realm of shunt active power filters.

The subsequent sections of this article unfold as follows: Section 2 expounds upon the system's structural framework. Section 3 outlines the presentation of the proposed control system. In Section 4, an extensive account of the simulation outcomes is provided, showcasing the preeminence of the BSC methodology and a comparative analysis is conducted against the PR controller. Ultimately, the conclusive insights are presented in Section 5.

2. SYSTEM STRUCTURE

Fig. 1(a) illustrates the configuration of the employed three-phase four-wire system within this research endeavor. At the point of common coupling (PCC), nonlinear loads are

interconnected. Facilitating the mitigation of both current imbalances and harmonics, the active power filter incorporates a quadruple-wire design. To counteract the harmonics, present in the inverter's output signal stemming from switching frequencies and their multiples a necessary inclusion is a filter positioned at the inverter's output. Specifically, the chosen filter variant is the LCL filter due to its favorable characteristics. Compared to L or LC counterparts, LCL filters exhibit superior harmonic suppression capabilities. Moreover, they offer heightened dynamic responsiveness, adaptability to low switching frequencies, reduced voltage droop, and enhanced damping. Furthermore, the adoption of LCL filters often incurs lower costs, attributed to the utilization of more compact inductors compared to L filters.

Depicted in Fig. 1(b) is the circuit diagram of a three-phase 4-wire system. The entities shown in this figure include L_I, L_g, and C_f, corresponding to the inverter side inductor, grid side inductor, and filter capacitor, respectively.

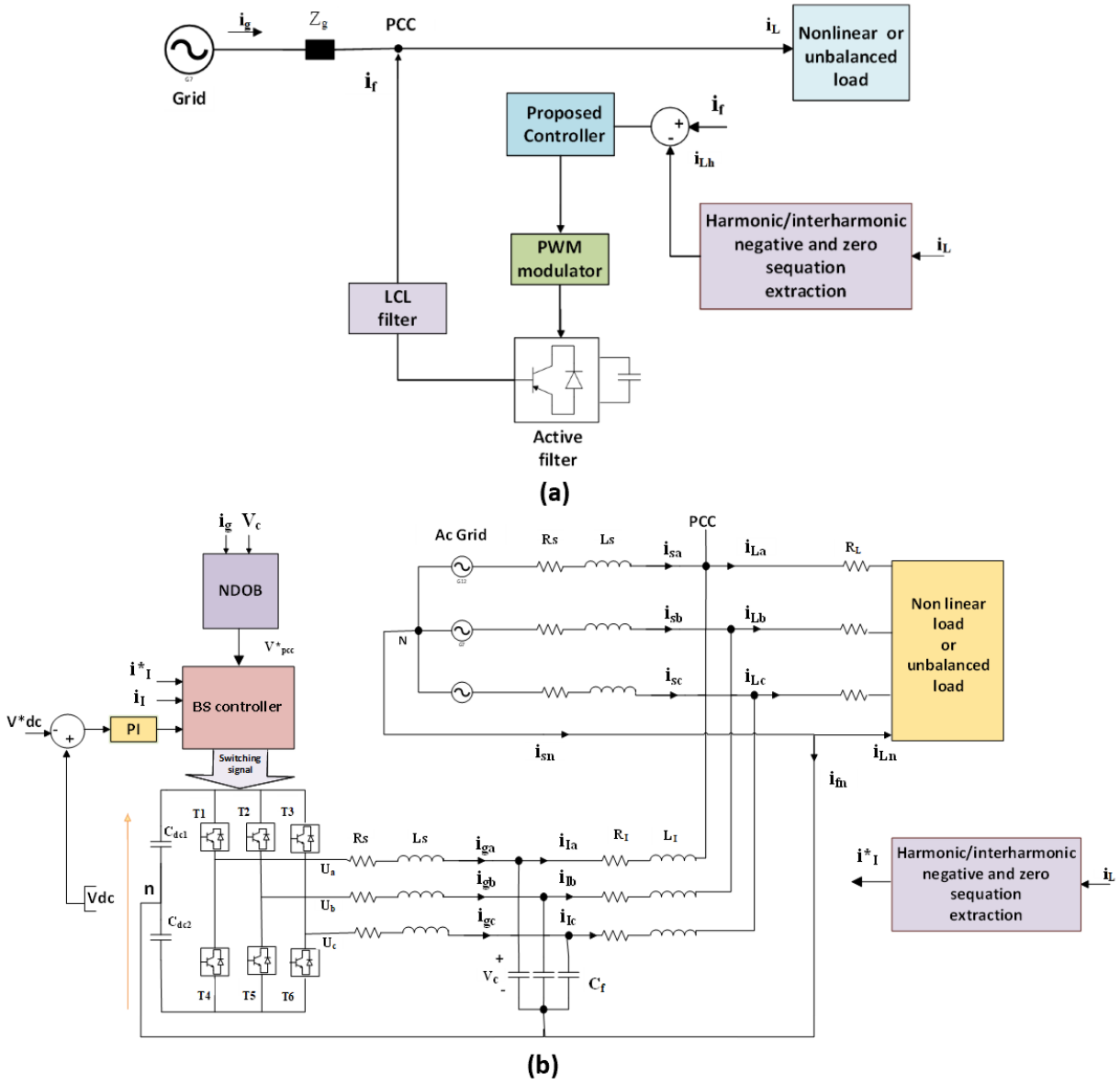

Fig. 1. a) Topology of the studied system; b) circuit diagram of a three-phase four-wire SAPF.

Also, R_I and R_g represent the associated parasitic resistances. Additionally, L_s and R_s represent the inductance and resistance of the grid impedance, respectively. Employing a synchronous reference frame, the reference current is derived, encompassing components related to harmonics, interharmonics, and load current imbalances.

3. THE PROPOSED CONTROL SYSTEM

The majority of techniques put forth for addressing harmonic distortions, including widely recognized methods like the PI and PR approaches, exhibit limitations in effectively countering interharmonics. In contrast, the backstepping method not only enables the mitigation of harmonic and interharmonic constituents in nonlinear systems but also extends its capability to address negative and zero sequence components. In the subsequent sections, we delve into the presentation of the backstepping method alongside the nonlinear NDOB method. Notably, these methods offer substantially heightened efficiency, as substantiated by forthcoming discussions.

3.1. Backstepping Controller

The backstepping control method remains a recursive design approach for nonlinear systems, serving the aims of stabilization and reference tracking. The central idea of the BS method entails considering certain state variables as "virtual controls." Control laws are then shaped using Lyapunov functions to ensure system stability. Within this section, a backstepping controller is crafted for an APF, ensuring accurate tracking of reference current. The stability of the closed loop system is established through Lyapunov analysis. The subsequent content delineates the sequential design procedure of the backstepping controller.

By employing Kirchhoff's rules to the arrangement depicted in Fig. 1(b), the equations governing the filter within the abc frame are derived as follows:

$$\begin{aligned} L_I \frac{d}{dt} i_I(t) + R_I i_I(t) &= u(t) - v_c(t) \\ C \frac{d}{dt} v_c(t) &= i_I(t) - i_g(t) \\ L_g \frac{d}{dt} i_g(t) + R_g i_g(t) &= v_c(t) - v_{pcc}(t) \end{aligned} \tag{1}$$

where i_I is the three-phase current of the inverter side filter, i_g is the three-phase current of the grid side filter, v_c is the voltages of the three-phase LCL filter capacitor referred to as point *N*, and u is the output voltage of the inverter.

State variables and control signals are defined as:

$$[x_1\ x_2\ x_3\ u] = \left[i_g\ v_c\ i_I\ u\right] \tag{2}$$

Therefore, we have

$$\begin{aligned} \dot{x}_1 &= \frac{1}{L_g} x_2 - \frac{R_g}{L_g} x_1 - \frac{v_{pcc}}{L_g} \\ \dot{x}_2 &= \frac{1}{c} x_3 - \frac{1}{c} x_1 \\ \dot{x}_3 &= \frac{1}{L_I} u - \frac{1}{L_I} x_2 - \frac{R_I}{L_I} x_3 \end{aligned} \tag{3}$$

Since v_{pcc} is neither a state variable nor a control input, it is considered as a disturbance:

$$d = -\frac{v_{pcc}}{L_g} \tag{4}$$

So, Eq. (3) could be rewritten as:

$$\begin{aligned} \dot{x}_1 &= \frac{1}{L_g} x_2 - \frac{R_g}{L_g} x_1 + d \\ \dot{x}_2 &= \frac{1}{c} x_3 - \frac{1}{c} x_1 \\ \dot{x}_3 &= \frac{1}{L_I} u - \frac{1}{L_I} x_2 - \frac{R_I}{L_I} x_3 \end{aligned} \tag{5}$$

3.2. Design of Nonlinear Disturbance Observer

To diminish the influence of disturbances and errors resulting from measurements, the NDOB approach is recommended for disturbance estimation. Take into account a nonlinear system defined as follows:

$$\begin{cases} \dot{x} = f(x) + g(x)u + h(x)d \\ y = k(x) \end{cases} \quad (6)$$

If the disturbance d is bounded and has slow change with time:

$$\begin{cases} |d| < \mu \\ \dot{d} \approx 0 \end{cases} \quad (7)$$

The technique employed for estimating the disturbance relies upon the fundamental NDOB method as outlined in reference [44]. However, in scenarios involving a periodic disturbance, it is advisable to employ the adapted NDOB method introduced in [45]. According to this approach, when the disturbance stems from a linear exogenous system:

$$\begin{cases} \dot{\xi} = A\xi \\ d = C\xi \end{cases} \quad (8)$$

where $\xi \in R^m$ and $d \in R$.

$$\begin{cases} \dot{z} = (A - l(x)h(x)C)z + Ap(x) - l(x)(h(x)Cp(x) + f(x) + g(x)u) \\ \hat{\xi} = z + p(x) \\ \hat{d} = C\hat{\xi} \end{cases} \quad (9)$$

where $z \in R^m$is the internal state variables of the NDOB and $p(x) \in R^m$ is a nonlinear function to be designed and usually is chosen as:

$$p(x) = kL_f^{r-1}h(x) \quad (10)$$

where L_f denotes Lie derivatives [46] and $k = [k_1 \ ... \ k_m]'$ are gains to be determined that k> 0.

The observer gain function *l(x)* is determined by:

$$l(x) = \frac{dp(x)}{dx} \quad (11)$$

Now, by implementing the modified NDOB method, disturbance in Eq. (5) can be estimated. Since the disturbance, $d = -\frac{v_{pcc}}{L_g}$, is a sinusoidal variable, it can be considered as follows:

$$d = E\sin(\omega t + \varphi), E = -\frac{|v_{pcc}|}{L_g} \quad (12)$$

According to Eq. (8), we can choose ξ as:

$$\begin{cases} \xi_1 = E\sin(\omega t + \varphi) \\ \xi_2 = E\cos(\omega t + \varphi) \end{cases} \quad (13)$$

By derivation of Eq. (13), the following equation is derived.

$$\begin{cases} \dot{\xi}_1 = E\omega\cos(\omega t + \varphi) \\ \dot{\xi}_2 = -E\omega\sin(\omega t + \varphi) \end{cases} \quad (14)$$

So

$$\begin{cases} \dot{\xi}_1 = \omega\xi_2 \\ \dot{\xi}_2 = -\omega\xi_1 \end{cases} \quad (15)$$

By comparing Eq. (15) with Eq. (8), the following equation could be derived.

$$A = \begin{bmatrix} 0 & \omega \\ -\omega & 0 \end{bmatrix}$$

$$C=[1 \quad 0] \tag{16}$$

Following the design procedure, the nonlinear variable *p(x)* can be chosen as:

$$p(x) = kL_f h(x) = kx_1 \tag{17}$$

where $k = \begin{bmatrix} k_1 \\ k_2 \end{bmatrix}$ and must be chosen, and it is selected based on [45].

$$l(x) = \begin{bmatrix} k_1 \\ k_2 \end{bmatrix} \tag{18}$$

Finally, by substituting these variables in Eq. (9) estimated disturbance is obtained with:

$$\begin{cases} \begin{bmatrix} \dot{z_1} \\ \dot{z_2} \end{bmatrix} = \begin{bmatrix} -k_1 & \omega \\ -\omega - k_2 & 0 \end{bmatrix} \begin{bmatrix} z_1 \\ z_2 \end{bmatrix} + \begin{bmatrix} \omega k_2 x_1 - k_1 (k x_1 + \frac{1}{L_g} x_2 - \frac{R_g}{L_g} x_1) \\ -\omega k_2 x_1 - k_2 (k x_1 + \frac{1}{L_g} x_2 - \frac{R_g}{L_g} x_1) \end{bmatrix} \\ \begin{bmatrix} \hat{\xi}_1 \\ \hat{\xi}_2 \end{bmatrix} = \begin{bmatrix} z_1 \\ z_2 \end{bmatrix} + \begin{bmatrix} k_1 \\ k_2 \end{bmatrix} x_1 \\ \hat{d} = [1 \quad 0] \begin{bmatrix} \hat{\xi}_1 \\ \hat{\xi}_2 \end{bmatrix} \end{cases} \tag{19}$$

3.3. Backstepping Control with NDOB Design

Through the use of BS, the higher order system is reconfigured into multiple first order subsystems via the incorporation of virtual controls. Within this arrangement, the objective revolves around attaining the desired filter current (x^*) value. Consequently, the emphasis lies in minimizing the disparity between the actual and intended values. Adhering to the design tenets of BS, the following relationship emerges:

3.3.1. First Stage

The tracking error for the first variable is defined as:

$$e_1 = x_1 - x^* \tag{20}$$

By derivation of Eq. (20), and subsequently substituting Eq. (5), the resultant expression is derived as follows:

$$\dot{e_1} = \dot{x_1} - \dot{x}^* = \frac{1}{L_g} x_2 - \frac{R_g}{L_g} x_1 + d - \dot{x}^* \tag{21}$$

The Lyapunov function is defined as:

$$V_1 = \frac{1}{2} {e_1}^2 \tag{22}$$

and its derivative is:

$$\dot{V_1} = \dot{e_1} e_1 = e_1 (\frac{1}{L_g} x_2 - \frac{R_g}{L_g} x_1 + d - \dot{x}^*) \tag{23}$$

In this regard, x_2 is the virtual control, and its ideal value is defined as Q_1, to ensure the stability of the system by the Lyapunov method, $\dot{V_1}$<0. so Q_1 is chosen as:

$$Q_1 = L_g (-d + \frac{R_g}{L_g} x_1 + H_1 e_1 + \dot{x}^*) \tag{24}$$

As a result:

$$\dot{V_1} = H_1 {e_1}^2 \leq 0 \tag{25}$$

By selecting a negative value for H_1, V_1>0, , $\dot{V_1}$<0 and according to Lyapunov's method, e_1 converges to zero and as a result, x_1 converges to x^*.

3.3.2. Second Stage

The error between real and ideal x_2 is considered:

$$e_2 = x_2 - Q_1 \tag{26}$$

The Lyapunov function is selected:

$$V_2 = \frac{1}{2}{e_1}^2 + \frac{1}{2}{e_2}^2 \tag{27}$$

where its derivation is as follows:

$$\dot{V_2} = \dot{e_1}e_1 + \dot{e_2}e_2 = \left(\frac{1}{L_g}x_2 + d - \frac{R_g}{L_g}x_1 - \dot{x}^*\right)e_1 + e_2\left(\dot{x}_2 - \dot{Q}_1\right) = \left(\frac{1}{L_g}(e_2 + Q_1) + d - \frac{R_g}{L_g}x_1 - \dot{x}^*\right)e_1 + e_2\left(\frac{1}{c}x_3 - \frac{1}{c}x_1 - \dot{Q}_1\right) \tag{28}$$

By substituting Eq. (25) in Eq. (28):

$$\dot{V_2} = H_1{e_1}^2 + e_1\frac{1}{L_g}e_2 + e_2(-\frac{1}{c}x_1 + \frac{1}{C}x_3 - \dot{Q}_1) \tag{29}$$

In Eq. (29), x_3 is a virtual input and its ideal value is defined by Q_2. To ensure the stability of the system by the Lyapunov method, $\dot{V_2}$<0, we define Q_2 as the ideal value of x_3:

$$Q_2 = c(\frac{1}{c}x_1 + H_2e_2 + \frac{1}{L_g}e_1 + \dot{Q}_1) \tag{30}$$

As a result:

$$\dot{V_2} = H_1{e_1}^2 + H_2{e_2}^2 \leq 0 \tag{31}$$

By selecting a negative value for H_2, V_2>0 and $\dot{V_2}$<0

3.3.3. Third Stage

The error between real and ideal x_3 is considered:

$$e_3 = x_3 - Q_2 \tag{32}$$

The Lyapunov function is selected:

$$V_3 = +\frac{1}{2}{e_1}^2 + \frac{1}{2}{e_2}^2 + \frac{1}{2}{e_3}^2 \tag{33}$$

where its derivation is as follows:

$$\dot{V_3} = \dot{e_1}e_1 + \dot{e_2}e_2 + \dot{e_2}e_2 = H_1{e_1}^2 + H_2{e_2}^2 + e_2\frac{1}{C}e_3 + e_3\left(\dot{x}_3 - \dot{Q}_2\right) = H_1{e_1}^2 + H_2{e_2}^2 + e_2\frac{1}{C}e_3 + e_3\left(\frac{1}{L_I}u - \frac{1}{L_I}x_2 - \frac{R_I}{L_I}x_3 - \dot{Q}_2\right) \tag{34}$$

Finally, the control signal u is obtained as:

$$u = L_I(\frac{1}{L_I}x_2 + \frac{R_I}{L_I}x_3 + H_3e_3 - \frac{1}{C}e_2 + \dot{Q}_2) \tag{35}$$

By substituting Eq. (35) in Eq. (34):

$$\dot{V_3} = H_1{e_1}^2 + H_2{e_2}^2 + H_3{e_3}^2 \leq 0 \tag{36}$$

Therefore, by choosing a negative value for H_3, V_3> 0, and $\dot{V_3}$<0, and according to Lyapunov's theorem, the stability of the system is guaranteed.

As can be seen, the control signal u contains $\dot{Q}_2$, which is the second derivative of v_{pcc}. This holds significant importance as even a minor measurement inaccuracy could magnify into a substantial error during differentiation. Hence, there exists a substantial anticipation that employing the NDOB method for estimating this measure would rectify the error effectively, consequently augmenting the compensation's overall accuracy.

4. SIMULATION RESULTS

To evaluate the effectiveness of the proposed approach, the MATLAB/Simulink simulation environment is employed to replicate the system depicted in Fig. 1(b). Essential

power system and control parameters can be found in Table 1. A comparative analysis is performed between the BS and PR methods to demonstrate the former's superior performance. Further insights into the linear method with the PR controller and RC method are provided in appendix A and appendix B, respectively.

Initially, the NDOB method is utilized to estimate the PCC voltage. The alignment between the actual and estimated voltages is clearly depicted in Fig. 2(a), showcasing the precision of the estimation process. This alignment indicates a highly accurate estimation. The error between the actual and estimated voltages is shown in Fig. 2(b), which is negligible in the steady state condition. Consequently, the estimated v_{pcc} is adopted for subsequent analysis in place of the measured v_{pcc}. In the following, an exploration of the PR and BS methods is conducted under diverse conditions. These conditions encompass scenarios involving harmonic and interharmonic loads, unbalanced load conditions, and instances of a weak grid.

Table 1. Simulation parameters.

Quality	Parameter	Value
AC power grid	Grid voltage (line-line RMS)	173 V
	Line frequency	50 Hz
	Grid impedance L_s/R_s	1.2 mH / 0.1 Ω
Load parameters	Linear load R_L	5 Ω
	Nonlinear load R/L	10 Ω /10 mH
LCL Filter parameters	Grid side impedance R_g/L_g	0.2 Ω / 5 mH
	Inverter side impedance R_I/L_I	0.2 Ω / 5 mH
	Filter capacitor C	5 µF
DC link voltage	DC link reference voltage V_{dc}	300 V
	DC link capacitor C_{dc1}, C_{dc2}	220 µF
	Switching Frequency f_{sw}	10 kHz
PI controller	k_p	0.2
	k_I	10
NDOB parameters	k_1 , k_2	200
BS parameters	H_1	-5e^4
	H_2	-1e^{-1}
	H_3	-9e^5

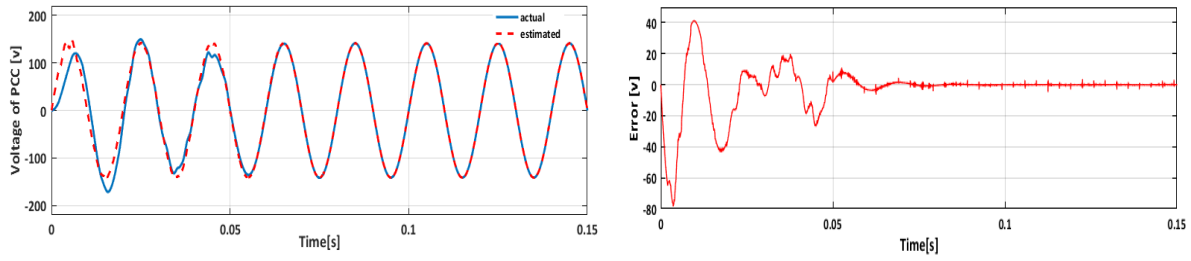

(a) (b)

Fig. 2. Performance of the disturbance observer: a) comparison of actual and estimated voltage of PCC; b) estimation error.

4.1. Presence of Harmonic Load

Within this section, an in-depth examination of the BS controller's performance is undertaken in the presence of a harmonic load. The configuration involves a nonlinear load

comprised of a six-pulse rectifier in tandem with an inductor and resistor, interconnected with the PCC. The load current waveform is presented in Fig. 3(a).

Notably, the load current exhibits a total harmonic distortion (THD) of 26%, which passes through the grid. Fig. 3(b) shows that the grid current experiences distortion until the instant t = 0.1s. The BS controller is invoked into action at this precise moment, i.e., t = 0.1s. Remarkably, the harmonic current stemming from the load is adeptly counteracted by the filter, resulting in a discernible enhancement in the waveform of the grid current. This transition is visually apparent in the plot. Fig. 3(c) showcases the waveform of the current introduced by the filter, leading to a substantial decrease in the THD of the grid current from 26.6% to a mere 1.02%.

In order to establish a comprehensive comparison, an examination of the PR method is also undertaken within the same operational context. The outcomes of this simulation endeavor are thoughtfully depicted in Fig. 4. Notably, in Fig. 4(a), a discernible shift in the grid current is observed after the activation of the PR controller at t = 0.1s. This adjustment contributes to a modest improvement in the grid current waveform, ultimately reducing THD to 4.9%. Fig. 4(b) showcases the waveform of the current introduced by the filter.

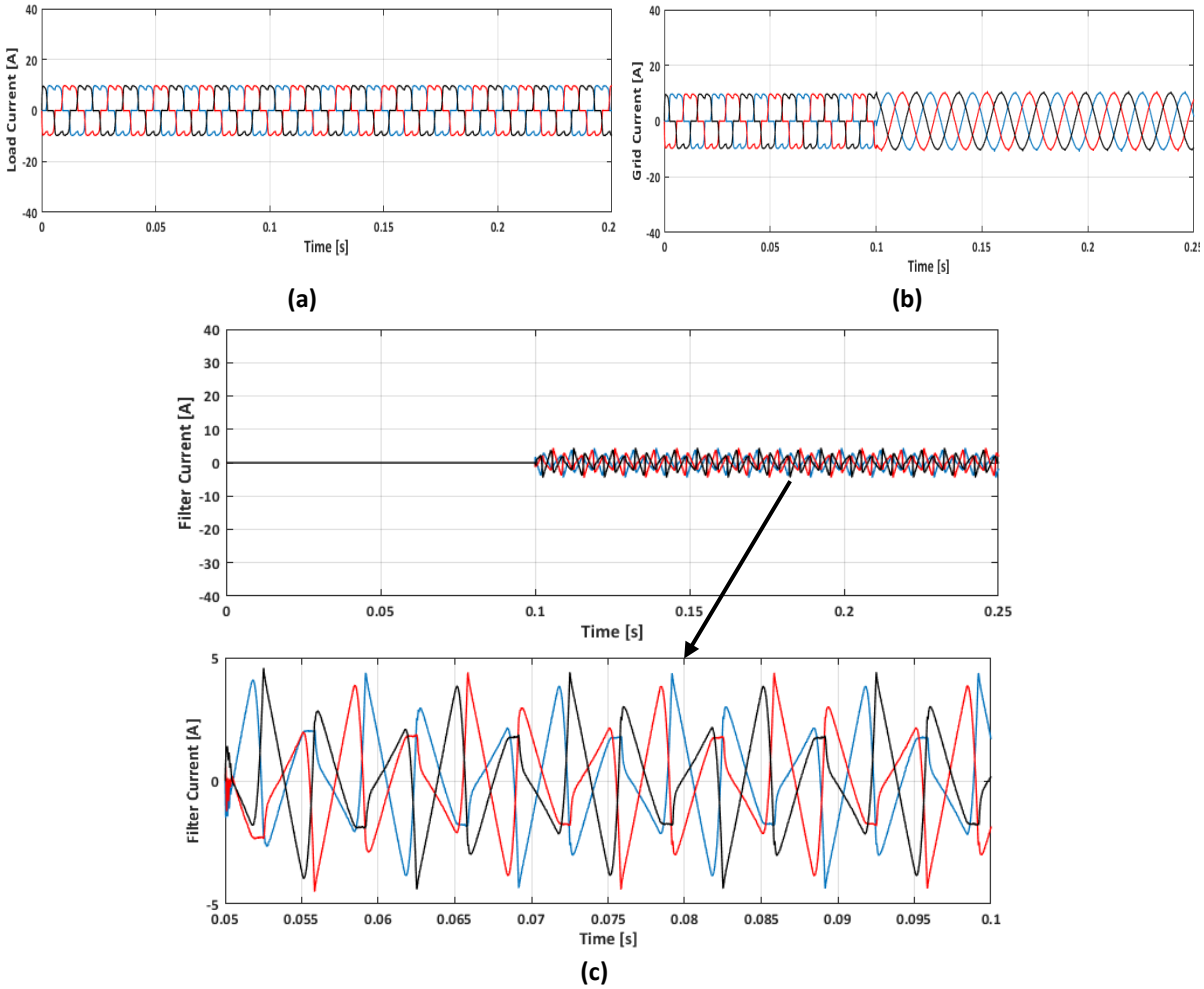

Fig. 3. Performance of the BS controller in the presence of harmonic load: a) load currents; b) grid currents; c) filter current.

To highlight the performance of the BS controller, the RC method was also subjected to investigation within the same conditions. Fig. 5(a) illustrates the changes in the grid current prior to and post compensation at t=0.1s. The current of the filter is shown in Fig. 5 (b). The RC method has reduced the THD to 4.5%, showing promising results.

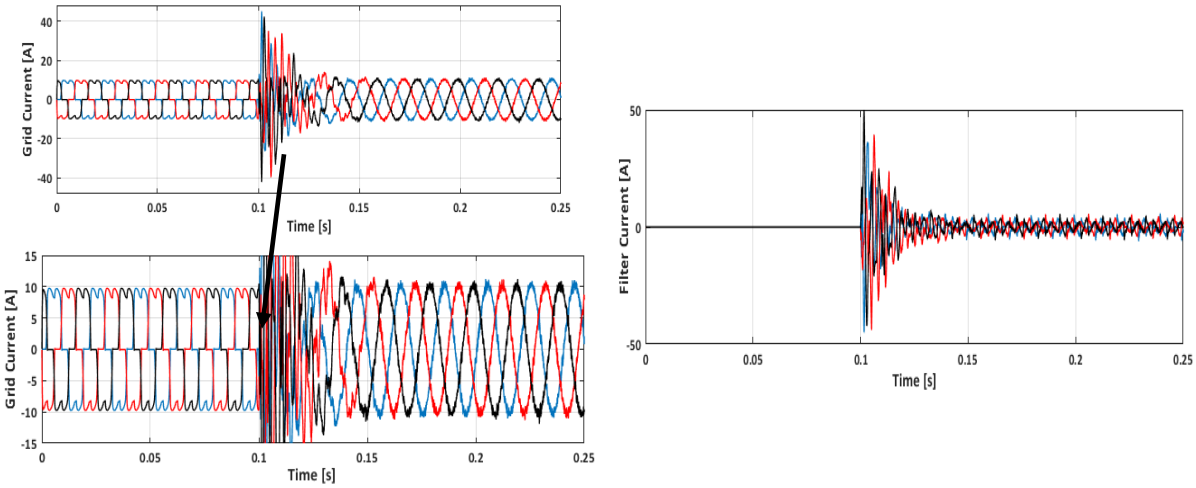

Fig. 4. Performance of the PR controller in the presence of harmonic load: a) grid currents; b) filter current.

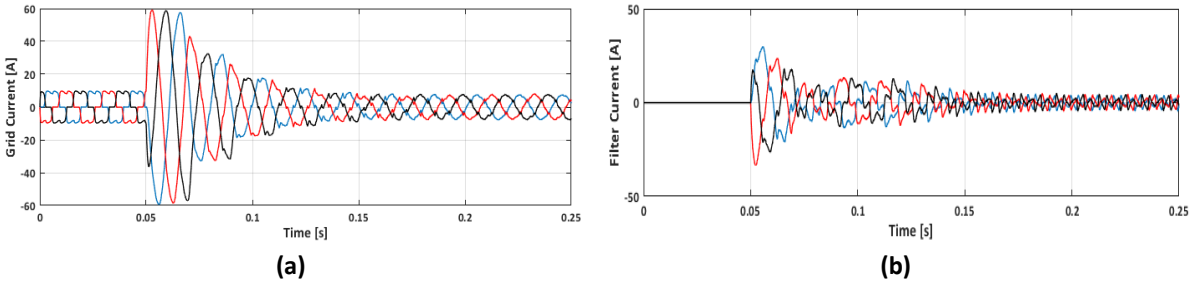

Fig. 5. Performance of the RC controller in the presence of harmonic load: a) grid current; b) filter current.

A discernible observation can be drawn from the comparative analysis of Fig. 3(b), Fig. 4(a) and Fig. 5(a): the transient response achieved through the implementation of the BS controller notably surpasses that of the alternative. This enhanced smoothness in the transient response serves as an additional advantageous aspect attributable to the BS controller. This juxtaposition of results effectively underscores the pronounced superiority of the BS method over the conventional PR and RC controller in the context of a harmonic load scenario.

4.2. Presence of Interharmonic Load

In this section, we examine the BS controller's performance amidst the presence of a load containing interharmonics. The experimental setup involves coupling an induction motor operating under a speed-controlled drive configuration, known for generating interharmonics, to the PCC [2]. Fig. 6(a) depicts the load current's temporal variation. Notably, at t=0.1s, the BS controller is initiated, prompting an observable shift in the subsequent grid current behavior. Fig. 6(b) details the comparative profiles of the grid current pre and post compensation, accompanied by the concurrent current contribution from the filtering system as illustrated in Fig. 6(c). The assessment of THD applied to the grid current is presented in Fig. 6(d), revealing a noteworthy reduction from an initial 33% to a significantly improved 0.7%.

In order to establish a comprehensive comparison, the PR method was also subjected to investigation within the same conditions. The outcomes of this analysis are presented in Fig. 7. Upon activation at t=0.1s, the PR controller's impact is visually illustrated in Fig. 7(a), which showcases the alteration in grid current prior to and post compensation. The

corresponding THD evaluations of the grid current are depicted in Fig. 7(b), highlighting a noteworthy decrease from the initial 33% to a diminished 9.21%.

To emphasize the performance of the BS controller, we conducted a comparative investigation with the RC method under identical conditions. Fig. 8(a) illustrates the alteration in grid current both before and after compensation at t=0.1s. Corresponding THD evaluations of the grid current are presented in Fig. 8(b). The RC method achieved a reduction in THD to 7.48%, showcasing promising efforts though falling short of the desired level. The fundamental operation of the RC method involves rejecting harmonics that are integer multiples of the main frequency. Consequently, the RC method may struggle to compensate for interharmonics in the load current.

Through this direct juxtaposition, it becomes evident that the BS method exhibits notably superior performance in the context of interharmonic compensation. This is substantiated by the drastic reduction of THD achieved through the BS approach, which effectively outperforms the PR method, underscoring its capability to significantly mitigate THD levels.

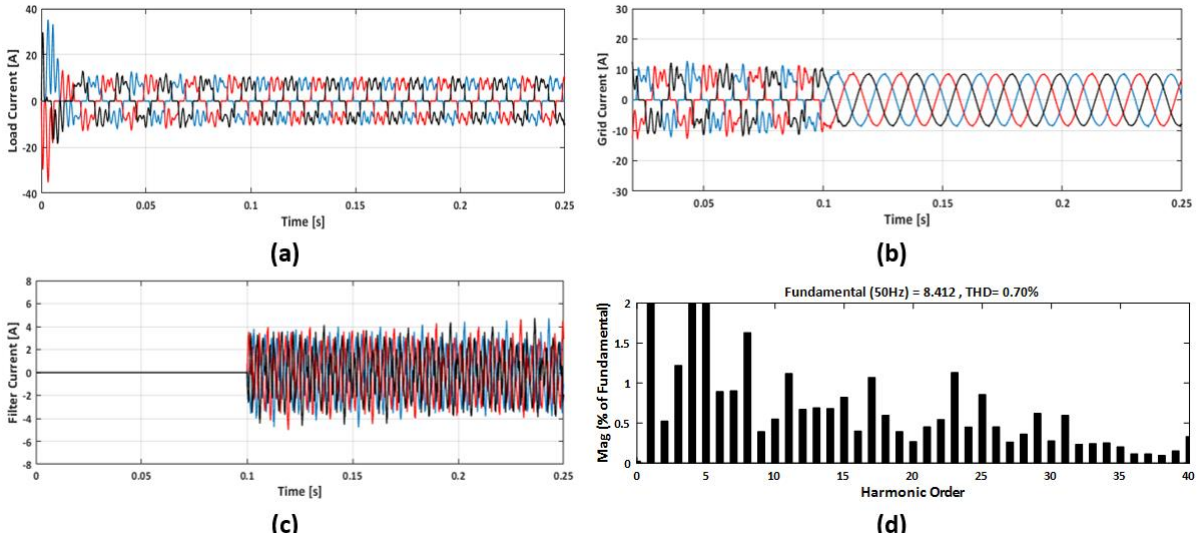

Fig. 6. Performance of the BS controller in the presence of interharmonic load: a) load currents; b) grid currents; c) filter current; d) THD analysis of grid current.

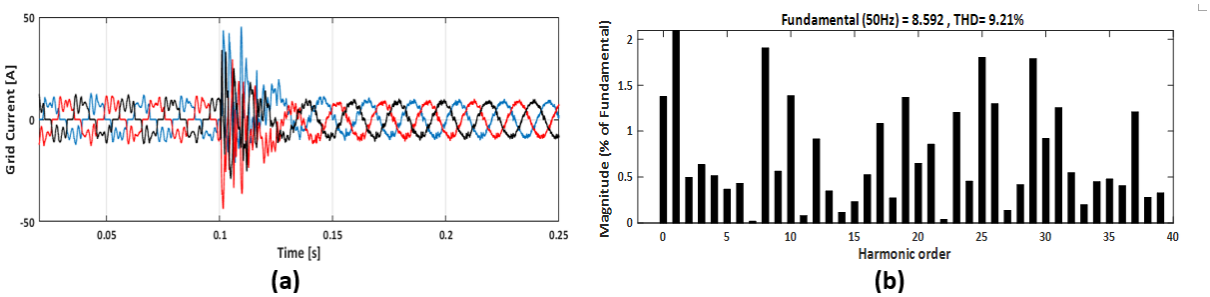

Fig. 7. Performance of the PR controller in the presence of interharmonic load: a) grid currents; b) THD analysis of the grid current.

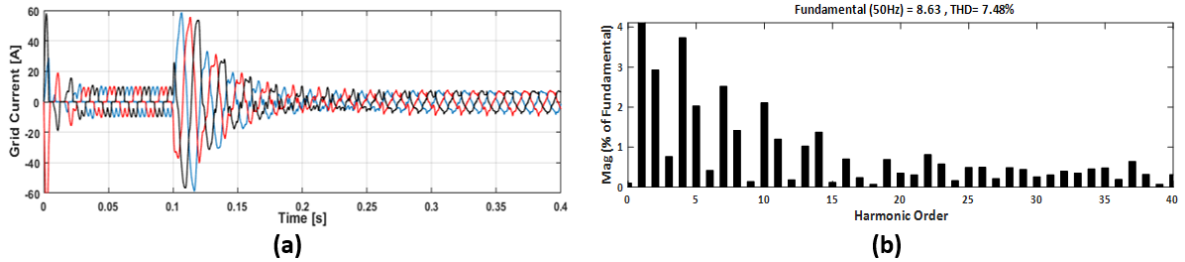

Fig. 8. RC controller performance in the presence of interharmonic load: a) grid currents; b) THD analysis of the grid current.

4.3. Performance under Polluted Grid

Within this section, the grid voltage demonstrates a departure from pure sinusoidal behavior, being imbued with harmonic constituents as depicted in Fig. 9(a). Notably, the fifth and seventh harmonic components constitute 10% and 7% of the fundamental component, respectively. Such harmonic presence in the grid voltage results in the distortion of the grid current, as visualized in Fig. 9(b), consequently yielding a THD value of 12%.

As seen in Fig. 9(b), upon the engagement of the BS controller at t=0.05s, a notable transformation transpires. The THD, initially measured at 12%, is observed to undergo a substantial reduction, culminating in an attenuated value of 0.5%. This outcome reinforces the efficacy of the BS intervention in rectifying grid current distortions induced by harmonic laden grid voltage conditions.

Figs. 9(c) and 9(d) depict the grid current after applying the PR and RC methods, respectively. While these methods are capable of compensating for harmonics, it is observed that they exhibit a slower transient response compared to the BS method.

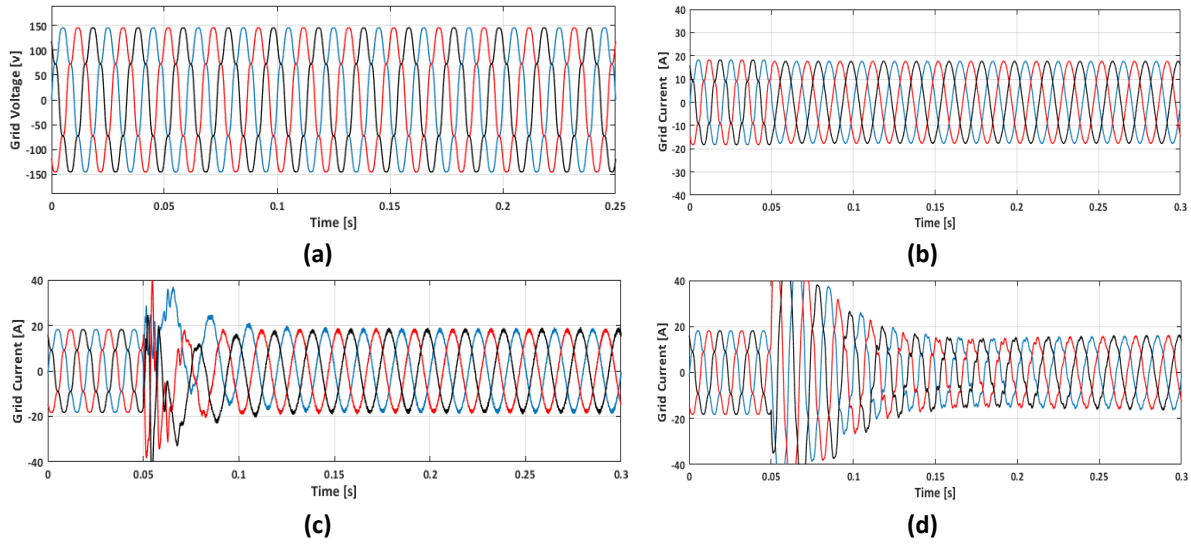

Fig. 9. Controller performance with the presence of harmonics in the grid voltage: a) grid voltage; b) grid current with BS; c) grid current with PR; d) grid current with RC.

4.4. Presence of Unbalanced Load

In this section, an unbalanced load (R1= 8Ω, R2= 12Ω, R3= 14Ω,) is connected to the PCC. Fig. 10(a) illustrates the load current profile, while the activation of the BS controller at t=0.1s is denoted. The response of the grid current before and after compensation is displayed in Fig. 10(b), effectively showcasing the influence of the compensation process with BS. Furthermore, Fig. 10(c) reveals the behavior of the neutral current, which notably converges to zero following the initiation of the BS.

To facilitate a comprehensive comparison, the PR and RC methods were also investigated. Upon activation at t=0.1s, the impact of the PR and RC controllers is visually illustrated in Fig. 10(d) and Fig. 10(e) respectively.

Despite promising efforts, it is evident that both PR and RC methods are unable to compensate for the unbalanced load current. This limitation arises from their ability to compensate only a limited number of harmonics, whereas the BS method proves capable of addressing all unwanted components.

This pattern emphasizes the successful control action of the BS controller in minimizing the neutral current contribution.

Based on this comprehensive analysis, a decisive conclusion can be drawn: the utilization of the BS method yields the potential to achieve a balanced and sinusoidal current on the grid side. Conversely, the PR method lacks this inherent capability. The distinctive configuration of the PR controller entails the necessity of individual controllers tailored to mitigate each harmonic component.

This design intricacy substantially amplifies the computational load. Additionally, the PR method falls short in effectively handling interharmonic constituents within the system. This drawback fundamentally distinguishes the PR controller-based approach from the BS method.

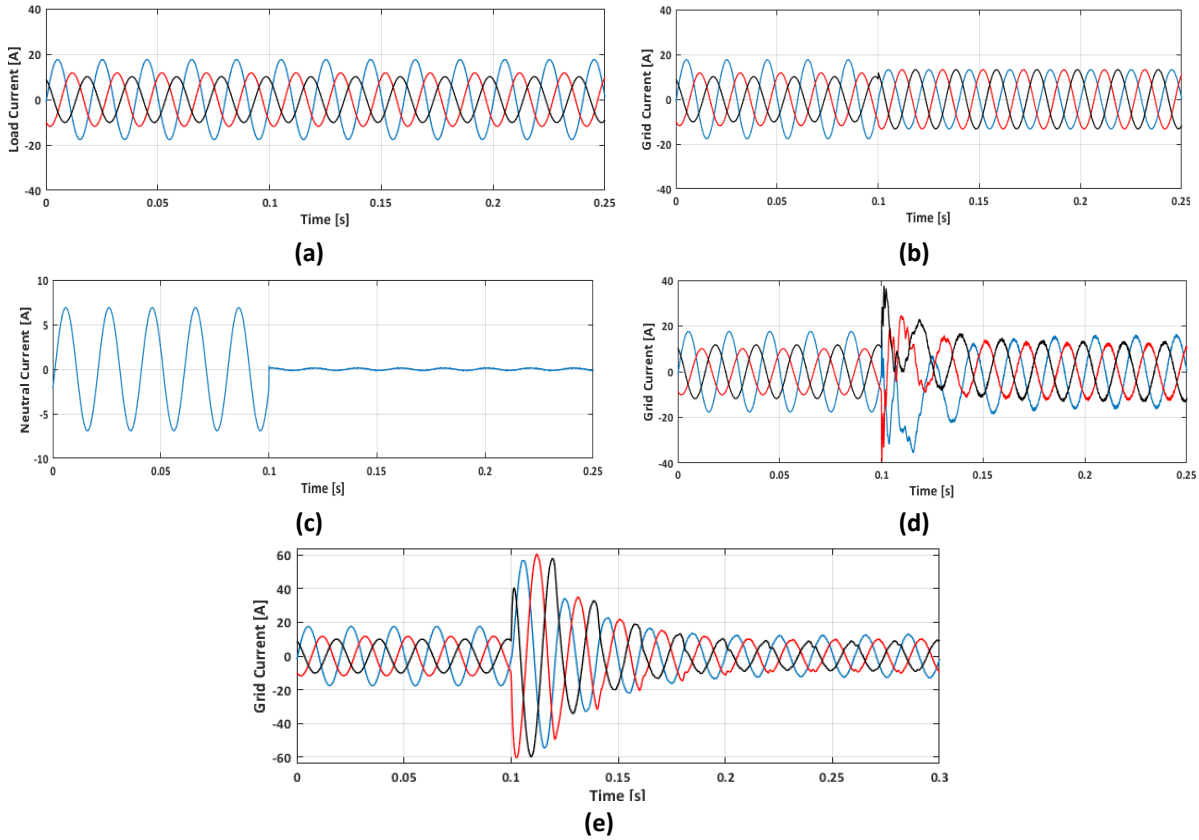

Fig. 10. Controllers' performance when the unbalanced load is connected to the PCC: a) load current; b) grid current with BSC; c) neutral current with BSC; d) grid current with PR; e) grid current with RC.

A salient feature of the BS method is its proficiency in compensating for a substantial number of harmonics. In stark contrast, the PR method selectively addresses only a limited set of harmonics. Furthermore, the BS method circumvents the need for crafting discrete controllers for each harmonic, thereby considerably alleviating the computational burden compared to the PR controller approach.

In contrast to the RC method, the BS approach eliminates the need for designing separate controllers. However, its performance relies on accurately compensating the main frequency component, resulting in challenges when effectively addressing inter-harmonic components in the system. Additionally, the RC method exhibits a slow response and is incapable of compensating for unbalanced current. These limitations are regarded as weaknesses when compared to the BS method. These advantageous characteristics distinctly positions the BS

method as a more efficient alternative to achieve harmonically cleaner grid currents. The summary of simulation results is given in Table 2.

Table 2. Comparison of the different techniques.

Grid current		Before compensation	BS with NDOB	PR	RC
THD%	Interharmonic load	33	0.7	9.21	7.48
	harmonic load	26	0.68	4.9	4.5
	Unbalanced load	–	✓	–	–
	Polluted grid	–	✓	✓	✓
The response time [s]			0	0.05	0.2

5. CONCLUSIONS

The present article introduces a control approach in managing the LCL filter-based SAPF within a four-wire system. This methodology incorporates a recursive backstepping strategy coupled with a nonlinear disturbance observer, aimed at ensuring a balanced grid current with minimal harmonic content. The proposed technique effectively addresses not only harmonics, but also interharmonics originating from nonlinear loads and a vulnerable grid. Notably, the method demonstrates competence in rectifying imbalances arising from single-phase or unbalanced three-phase loads. An integral feature of this approach is the integration of the NDOB, which enhances the robustness of the backstepping controller against system parameter uncertainties and external disruptions. Simulation outcomes notably underscore the superior attributes of the BS method in contrast to alternative techniques:

- Minimal parameter design is requisite, as the method obviates the need for discrete controllers catering to distinct harmonic components.
- Remarkably, the BS method excels not only in harmonic compensation, but also the eradication of interharmonic components—an accomplishment unattainable by prior methodologies.
- The rapid transient response further bolsters the appeal of the BS approach.
- The method's resilience to external disturbances and adeptness in handling parameter uncertainty is a testament to its robustness.
- A distinguishing asset of the BS method is its proficiency in effectively mitigating negative and zero sequence currents prompted by load imbalances, further enhancing its utility in real world scenarios.

The scope of future work could involve finding solutions for the following:

- In this research, the grid frequency is assumed to be constant. For future work, the effect of grid frequency deviation can be also considered.
- The cases conducted in this research can be replicated in a laboratory environment to validate the accuracy of this method through experimental results.

APPENDIX A: THE PR CONTROLLER

In inverter applications, designing controllers for sinusoidal signals is complex due to the need for precise gain adjustments to manage fundamental frequencies and harmonics. The PR controller has gained popularity as it addresses two key issues of conventional PI

controllers: achieving zero steady state error with sinusoidal references and effectively injecting disturbances. The transfer function of the proportional-resonance controller is presented as follows:

$$G_s = k_p + \sum_{h=1,5,7,11,13} \frac{2k_{Rh}\omega_c s}{s^2+2k_{Rh}\omega_c s+(h\omega_f)^2} \quad \text{(A-1)}$$

where k_p is the proportional gain, k_{Rh} is the resonant gain and ω_c is the cut-off frequency. The parameters that need to be tuned are k_p, ω_c and k_{Rh} $(h = 1,5,7,11,13)$. The system stability has been ensured through analysis of its loop gain bode diagram (depicted in Fig. A1). By calculating the phase margin (PM) and gain margin (GM), parameters conducive to system stability have been determined, as outlined in Table A1. Fig. A1 substantiates this by demonstrating PM exceeding 30 degrees, GM being greater than zero, and a crossover frequency of 1540Hz. Hence, the system stability is affirmed.

Table A-1. PR controller parameters.

Parameter	Value
k_p	6.2
ω_c	8 rad/s
k_{Rh} (h=1)	600
k_{Rh} (h=5)	340
k_{Rh} (h=7)	540
k_{Rh} (11,13)	800

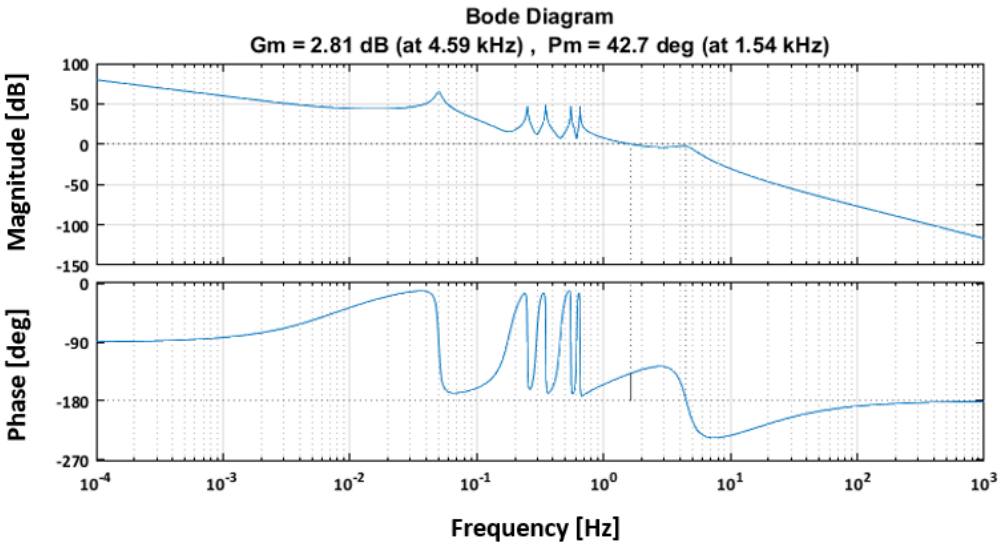

Fig. A-1. Open-loop frequency response for the control loop with PR controller.

APPENDIX B: THE RC METHOD

The performance of the RC method is based on IMP. In this way, RC can track harmonics with high accuracy by creating high gains in the harmonic frequencies of the input signal. This feature is very efficient for current harmonic compensation by APF. Fig. B1 shows the plug-in RC closed loop control system.

where $R(z)$ is the reference input, $G_p(z)$ is the basic plant, $G_c(z)$ is the conventional feedback controller (PI controller). k_r is the gain of RC and is a positive constant $0 \leq k_r \leq 1$ [47]. $G_f(z)$, is a phase lead compensation filter to stabilize the overall closed-loop system. $Q(z)$ is a low pass filter to increase the robustness of the system.

The transfer function of the plug-in repetitive controller is presented as follows:

$$G_r(z) = \frac{U_r(z)}{E(z)} = k_r \frac{z^{-N}\, Q(z)}{1 - z^{-N}\, Q(z)} G_f(z) \quad \text{(B-1)}$$

where $N = f_s/f$ that f is the fundamental frequency of the reference signal and f_s is the sampling frequency. It is clear that if $Q(z) = 1$, $G_r(z)$ at the harmonic's frequency reaches infinity and the tracking error becomes zero. $Q(z)$ has been implemented as a low-pass binomial FIR filter with no phase delay. ($Q(z) = 0.1z + 0.8 + 0.1z^{-1}$ and $G_f(z) = z^2$ is employed [47]).

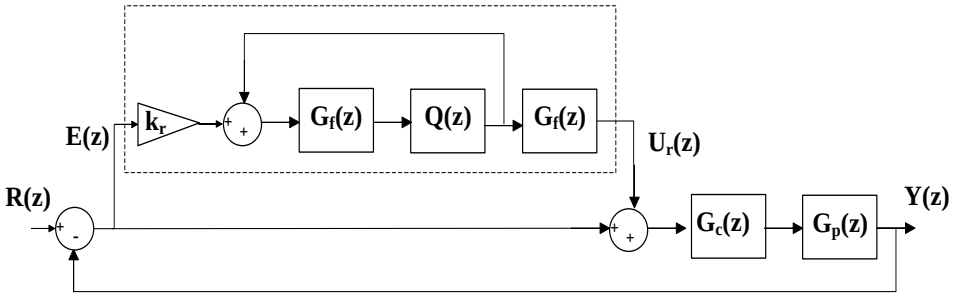

Fig. B-1. Plug-in repetitive control system.

The parameters that need to be tuned are k_p, k_I, k_r. The system stability has been ensured through analysis of its loop gain bode diagram (depicted in Fig. B2). By calculating the phase margin (PM) and gain margin (GM), parameters conducive to system stability have been determined, as outlined in Table B1. Fig. B2 substantiates this by demonstrating PM exceeding 25 degrees, GM being greater than zero, and a crossover frequency of 803Hz. Hence, the system stability is affirmed.

Table B-1. PR controller parameters.

Parameter	Value
k_r	0.8
k_p	2.2
k_I	10
N	200
f_s	10 kHz

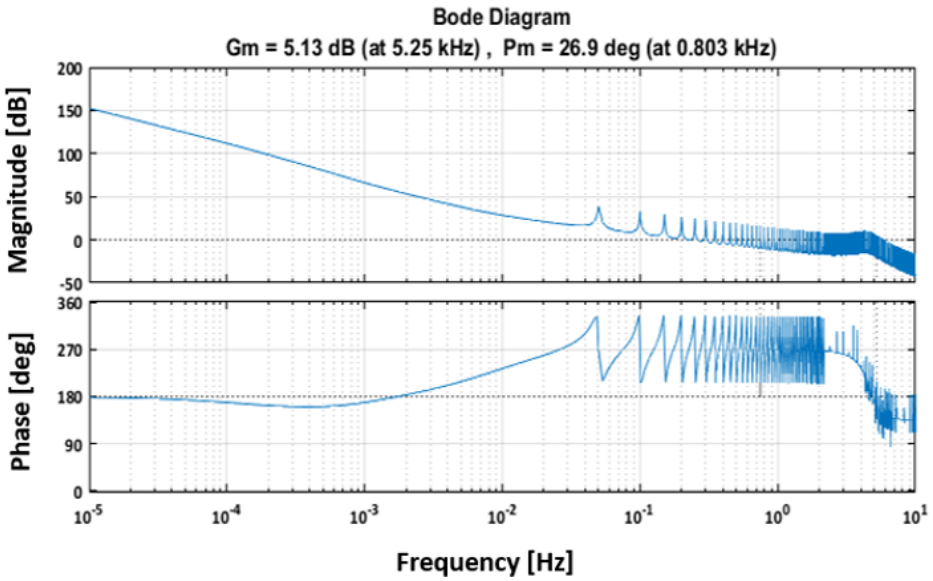

Fig. B-2. Open-loop frequency response for the control loop with repetitive controller.

REFERENCES

[1] M. Akram, R. Burch, G. Carpinelli, G. Chang, V. Dinavahi, C. Hatziadoniu, W. Grady, E. Gunther, M. Halpin, P. Lehn, Y. Liu, R. Langella, M. Lowenstein, A. Medina, T. Ortmeyer, S. Ranade, P. Ribeiro, N. Watson, J. Wikston, W. Xu, "Interharmonics: theory and measurement," *IEEE Transactions on Power Delivery*, vol. 22, no. 4, pp. 2335–2348, 2007, doi: 10.1109/TPWRD.2007.905505.

[2] F. Rosa, R. Langella, A. Sollazzo, A. Testa, "On the interharmonic components generated by adjustable speed drives," *IEEE Transactions on Power Delivery*, vol. 20, no. 4, pp. 2535–2543, 2005, doi: 10.1109/TPWRD.2005.852313.

[3] D. Li, K. Yang, Z. Zhu, Y. Qin, "A novel series power quality controller with reduced passive power filter," *IEEE Transactions on Industrial Electronics*, vol. 64, no. 1, pp. 773–784, 2017, doi: 10.1109/TIE.2016.2527727.

[4] T. Lee, S. Hu, "An active filter with resonant current control to suppress harmonic resonance in a distribution power system," *IEEE Journal of Emerging and Selected Topics in Power Electronics*, vol. 4, no. 1, pp. 198–209, 2016, doi: 10.1109/JESTPE.2015.2478149.

[5] E. Clarke, *Circuit Analysis AC Power Systems*, New York: John Wiley & Sons, 1950.

[6] C. Lascu, L. Asiminoaei, I. Boldea, F. Blaabjerg, "Frequency response analysis of current controllers for selective harmonic compensation in active power filters," *IEEE Transactions on Industrial Electronics*, vol. 56, no. 2, pp. 337-347, 2009, doi: 10.1109/TIE.2008.2006953.

[7] J. Fei, H. Wang, "Experimental investigation of recurrent neural network fractional-order sliding mode control of active power filter," *IEEE Transactions on Circuits and Systems*, vol. 8, no. 6, pp. 2522-2526, 2020, doi: 10.1109/TCSII.2019.2953223.

[8] H. Battista, R. Mantz, "Harmonic series compensators in power systems: their control via sliding mode,"*IEEE Control Systems Technology*, vol. 8, no. 6, pp. 939–947, 2000, doi: 10.1109/87.880597.

[9] L. Proença, L. Rolim "Two-leg modular multilevel cascade converter as active power filter control improvement," *IEEE Latin America Transactions*, vol. 17, no. 9, pp. 1501-1508, 2019, doi: 10.1109/TLA.2019.8931144.

[10] S. Bosch, J. Staiger, H. Steinhart, "Predictive crrent control for an active power filter with LCL-flter," *IEEE Transactions on Industrial Electronics*, vol. 65, no. 6, pp. 4943 - 4952, 2018, doi: 10.1109/TIE.2017.2772176.

[11] H. Chen, H. Liu, Y. Xing, H. Hu, "Enhanced DFT-based controller for selective harmonic compensation in active power filters," *IEEE Transactions on Power Electronics, vol*. 34, no. 8, pp. 8017-8030, 2018, doi: 10.1109/TPEL.2018.2877848.

[12] H. Geng, Z. Zheng, T. Zou, B. Chu, A. Chandra, "Fast repetitive control with harmonic correction loops for shunt active power filter applied in weak grid," *IEEE Transactions on Industry Applications,* vol. 55, no. 3, pp. 3198-3206, 2019, doi:10.1109/TIA.2019.2895570.

[13] W. Jiang, X. Ding, Y. Ni, J. Wang, L. Wang, W. Ma, "An improved deadbeat control for a three phase three line active power filter with current tracking error compensation," *IEEE Journal of Emerging and Selected Topics in Power Electronics*, vol. 33, no. 3, pp. 2061–2072, 2018, doi: 10.1109/TPEL.2017.2693325.

[14] W. Sou, W. Choi, C. Chao, C. Chi. Lam, C. Gong, C. Wong, M. Wong, "A deadbeat current controller of LC hybrid active power filter for power quality improvement," *IEEE Journal of Emerging and Selected Topics in Power Electronics*, vol. 8, pp. 3891-3905, 2020, doi: 10.1109/JESTPE.2019.2936397.

[15] T. Thentral, K. Vijayakumar, S. Usha, R. Palanisamy, T. Babu, H. Alhelou, A. Amer, "Development of control techniques using modified fuzzy based SAPF for power quality enhancement," *IEEE Access,* vol. 9, pp. 2169-3536, 2021, doi: 10.1109/ACCESS.2021.3077450.

[16] A. Testa, A. Koduah, F. Effah, "Fuzzy logic-controlled hybrid active filter for matrix converter input current harmonics," *Energies*, vol. 15, 7640, 2022, doi: 10.3390/en15207640.

[17] C. Chen, C. Chen, "Recurrent wavelet fuzzy neural network-based reference compensation current control strategy for shunt active power filter," *Energies*, vol. 15, 8687, 2022, doi: /10.3390/en15228687.

[18] P. Chittora, A. Singh, M. Singh, "Design and analysis of functional link artificial neural network controller for shunt compensation," *IET Generation, Transmission and Distribution*, vol. 13, no. 11, pp. 2280-2289, 2019, doi: 10.1049/iet-gtd.2018.6070.

[19] C. Xie, D. Liu, K. Li, J. Zou, K. Zhou, J. Guerrero, "Passivity-based design of repetitive controller for LCL-type grid-connected," *IEEE Transactions on PowerElectronic*, vol. 36, no. 2, pp. 2420–2431, 2021, doi: 10.1109/IPEMC-ECCEAsia48364.2020.9368176.

[20] M. Li, H. Xiao, M. Cheng, ''An adaptive strategy based on repetitive predictive control for improving adaptability of LCL type grid connected inverters under weak grid,'' *IEEE Transactions on Power Electronics*, vol. 37, no. 3, pp. 2562–2572, 2022, doi: 10.1109/TPEL.2021.3108878.

[21] M. Li, H, Xio, M. Cheng, ''An equivalent differential method for active damping of LCL type grid-connected inverters with grid-side inductor voltage feedback,'' *IEEE Transactions on Power Electronics*, vol. 38, no. 6, pp. 7009-7021, 2023, doi: 10.1109/TPEL.2023.3252163.

[22] Z. Chen, H. Zha, K. Peng, J. Yang, J. Yan, "A design method of optimal PID-based repetitive control systems," *IEEE Access*, vol. 8, pp. 139625–139633, 2020, doi: 10.1109/ACCESS.2020.3012506.

[23] Y. Wang, L. Zheng, H. Zhang, W. Zheng, "Fuzzy observer based repetitive tracking control for nonlinear systems," *IEEE Transactions on Fuzzy Systems*, vol. 28, no.10, pp. 2401–2415, 2020, doi: 10.1109/TFUZZ.2019.2936808.

[24] H. Lin, X. Guo, D. Chen, S. Wu, G. Chen, "A frequency adaptive repetitive control for active power filter with 380V/75A SiC-inverter," *IEEE Transactions on Industry Applications*. vol. *58*, pp. 5469–5479, 2022, doi: 10.1109/TIA.2022.3176848.

[25] Y. Chen, K. Zhou, C. Tang, Y. Shu, Y. Yang, "Fractional-order multiperiodic odd-harmonic repetitive control of programmable AC power sources," *IEEE Transactions on Power Electronics*, vol. 37, no. 7, pp. 7751-7758, 2022, doi: 10.1109/TPEL.2022.3147062.

[26] D. Liu, B. Huang, L. Liu, H. Wang, Y. Huang, "Frequency-adaptive virtual variable sampling-based repetitive control for active power filter," 4th International Conference on Smart Power and Internet Energy Systems, 2022, doi: 10.1109/SPIES55999.2022.10082719.

[27] M. Karbasforooshan, M. Monfared, "An improved reference current generation and digital deadbeat controller for single-phase shunt active power filters," *IEEE Transactions on Power Delivery*, vol. 35, no. 6, pp. 2663–2671, 2020, doi: 10.1109/TPWRD.2020.2974155.

[28] B. Wang, R. Zhang, G. Feng, U. Manandhar, G. Guo, ''Event triggered deadbeat predictive control for DC microgrid,'' 31st Australasian Universities Power Engineering Conference, 2021, doi:10.1109/TIE.2022.3201281.

[29] W. Sou, W. Choi, C. Chao, C. Lam, C. Gong, C. Wong, M. Wong, "A deadbeat current controller of LC hybrid active power filter for power quality improvement," *IEEE Journal of Emerging and Selected Topics in Power Electronics*, vol. 8, no. 4, pp. 3891-3905, 2019, doi: 10.1109/JESTPE.2019.2936397.

[30] J. Fei, Y. Chen, "Dynamic terminal sliding-mode control for single-phase active power filter using new feedback recurrent neural network," *IEEE Transactions on Power Electronics*, vol. 35, no. 9, pp. 9904–9922, 2020, doi: 10.1109/TPEL.2020.2974470.

[31] L. Liu, J. Fei, "Extended state observer-based interval type-2 fuzzy neural network sliding mode control with its application in active power filter," *IEEE Transactions on Power Electronics*, vol. 37, no. 3, pp 5138–5154, 2022, doi: 10.1109/TPEL.2021.3127896.

[32] F. Lin, S. Chen, M. Huang C. liang, "Adaptive complementary sliding mode control for synchronous reluctance motor with direct-axis current control," *IEEE Transactions on Industrial Electronics,* vol. 69, no. 1, pp. 141-150, 2022, doi: 10.1109/TIE.2021.3050373.

[33] J. Fei, L. Zhang, J. Zhuo, Y. Fang, "Wavelet fuzzy neural super-twisting sliding mode control of active power filter," *IEEE Transactions on Fuzzy Systems*, vol. 31, no. 11, 2023, doi:10.1109/TFUZZ.2023.3272028.

[34] L. Zhang, J. Fei, "Intelligent complementary terminal sliding mode using multiloop neural network for active power filter," *IEEE Transactions on Power Electronics*, vol. *38*, no. 8, pp. 9367–9383, 2023, doi: 10.1109/TPEL.2023.3266738.

[35] J. Yu, P. Shi, J. Liu, *Intelligent Backstepping Control for the Alternating-Current Drive Systems*, Studies in Systems, Decision and Control, Springer International Publishing, Cham, Switzerland, Springer Nature, 2021.

[36] X. Wang, D. Sun, Z. Zhu, "Resonant-based backstepping direct power control strategy for DFIG under both balanced and unbalanced grid conditions," *IEEE Transactions on Industry Applications*, vol. 53, no. 5, pp. 4821-4830, 2017, doi: 10.1109/ECCE.2016.7855399.

[37] A. Mahfouz, S. Zaid, S. Saad, A. Hagras, "Sensorless DC voltage control with backstepping design scheme for shunt active power filter," *Journal* of *Electrical Engineering*, vol. 15, no. 1, pp. 303–312, 2015, doi: api.semanticscholar.org/CorpusID:220485404.

[38] A. Ghamri, T. Mahni, M. Benchouia, K. Srairi, A. Golea, "Comparative study between different controllers used in three phase four wire shunt active filter," *Energy Procedia*, vol. 74, pp. 807–816, 2015, doi: 10.1016/j.egypro.2015.07.816.

[39] A. Martin, J. Cano, J. Silva, J. Vazquez, "Backstepping control of smart grid-connected distributed photovoltaic power supplies for telecom equipment," *IEEE Transactions on Energy Conversion*, vol. 30, no. 4, pp. 1496-1504, 2015, doi: 10.1109/TEC.2015.2431613.

[40] N. Debdouche, L. Zarour, H. Benbouhenni, F. Mehazzem, B. Deffaf, "Robust integral backstepping control microgrid connected photovoltaic System with battery energy storage through multi-functional voltage source inverter using direct power control SVM strategies," *Energy Reports,* vol. 10, pp. 565–580, 2023, doi: 10.1016/j.egyr.2023.07.012.

[41] D. Sun, X. Wang, Y. Fang, "Backstepping direct power control without phase-locked loop of AC/DC converter under both balanced and unbalanced grid conditions," *IET Power Electronics*, vol. 9, no. 8, pp. 1614-1624, 2016, doi: 10.1049/iet-pel.2015.0653.

[42] D. Xu, G. Wang, W. Yan, X. Yan, "A novel adaptive command-filtered backstepping sliding mode control for PV grid-connected system with energy storage," *Solar Energy*, vol. 178, pp. 222–230, 2019, doi: 10.1016/j.solener.2018.12.033.

[43] N. Dehkordi, N. Sadati, M. Hamzeh, "A robust backstepping high-order sliding mode control strategy for grid-connected DG units with harmonic interharmonic current compensation capability," *IEEE Transactions on Sustainable Energy*, vol. 8, no. 2, pp. 561-572, 2017, doi: 10.1109/TSTE.2016.2611383.

[44] J. Yang, W. Chen, S. Li, "Non-linear disturbance observer based robust control for systems with mismatched disturbances/uncertainties," *IET Control Theory and Applications*, vol. 5, no. 18, pp. 2053-2062, 2011, doi: 10.1049/iet-cta.2010.0616.

[45] W. Chen, "Disturbance observer based control for nonlinear systems," *IEEE/ASME Transactions on Mechatronics,* vol. 9, no. 4, pp. 706–710, 2004, doi: 10.1109/TMECH.2004.839034.

[46] A. Isidori, *An Introduction In Nonlinear Control Systems*, New York: Springer-Verlag, 1999.

[47] A. Garcia-Cerrada, O. Pinzon-Ardila, V. Feliu-Bat, P. Garcia-Gonzalez, "Application of a repetitive controller for a three phase active power filter," *IEEE Transactions on Power Electronics*, vol. 22, no. 1, pp. 237-246, 2007, doi10.1109/TPEL.2006.886609.